УДК 55.553.067
DOI 10.31242/2618-9712-2022-27-1-32-45

Volcanic features of IOCG mineralization in Kildyam volcanic complex of Central Yakutia (Russia)

A.V. Kostin

Diamond and Precious Metal Geology Institute SB RAS, Yakutsk, Russia
a.v.kostin2006@rambler.ru

Abstract. *This contribution presents the evidence for volcanic geology and associated magnetite-hematite and other mineralization from volatile-rich lavas and related gas-phases. Recently discovered the Yakut iron belt is approximately 120 km long and 10 km wide. The Zone contains 1 large and about 4 smaller high-grade ore deposits in the upper Jurassic sediments. The existence of ore with volcanic features demonstrates that ore magmas reach surface in Kildyam Volcanic Complex. Occurrence of rapid-growth textures, vesicular ore lava and pyroclastic ore demonstrate emplacement of ore magmas at or near the surface and confirm that this deposit is volcanic. Kildyam ore occur as massive, sub-horizontal, tabular bodies, as crosscutting feeder dikes and as stratified, fragmental magnetite-lavas material. Effusive iron-oxide liquids reach surface via feeder dikes and sub-parallel swarms of fissures and voids. Main ore product, expelled from fissure, is a magnetite-rich pyroclastic material deposited on Kildyam andesitic lavas. Heavy magnetite lava characterized by textures: (a) subrounded fragments of altered volcanic rocks in a magnetite matrix; (b) upward transition from dense to highly vesicular magnetite lava; (c) pyroclastic ore dominated by lapilli-sized material discordant above ore lava with sheeted structure; (d) magnetite lava with well-developed sheeted structure due to laminar flow; (e) scoriaceous magnetite lava from the flow top; (f) stratification in a lenses of pyroclastic ore within the magnetite lava flow. The final magnetite ore bodies formed from iron oxide magma that intruded local volcanic sequence and in places erupted at surface. Volcanic breccia and iron-oxide mineralization from Kildyam succession contain (a) oxides: hematite, magnetite, Ti-magnetite; phenocrysts of ilmenite, rutile, pseudorutile, and ilmenorutile (Ti,Nb,Fe+++)O_2; (b) sulfides: argentite, chalcopyrite, bartonite, pyrite, pyrrhotite, tetrahedrite, troilite; (c) alloys: Au, Au–Ag–Cu–Fe, Cu, Cu–Zn, Fe, Fe–Al–Cu. Ni–Fe–Cu–Sn. Iron native and as sulfides with copper, enriched from the liquid sulfide droplets; copper, led, silver and gold precipitated from high-temperature late magmatic fluids. The study presents evidence for growth of magnetite from iron-oxide-rich liquids and of magnetite, hematite and other minerals from volatile-rich magmas and related gas-phases. Occurrence of diverse gold, silver, copper and lead minerals in magnetite lavas led to preserve IOCG (Iron Oxide Copper Gold) mineralization. Based on the research carried out so far, it is generally accepted that Kildyam group has potential to become a new world-class size IOCG deposit at 30 km near Yakutsk.*

Keywords: Kildyam volcanic complex, liquid immiscibility, metallic alloys, IOCG mineralization, olivine-pyroxenite, andesite, dacite, melilitite, magnetite lavas, gold, silver.

Acknowledgements. *This research was funded by Diamond and Precious Metal Geology Institute, Siberian Branch of the Russian Academy of Sciences (project number 0381-2019-004). I am grateful for supporting the idea of studying the Kildyam volcanic complex and numerous discussions on all aspects of volcanism to my colleagues from the Institute – V.A. Trunilina, O.B. Oleynikov, V.S. Grinenko and M.S. Zhelonkina.*

Introduction

Geological conceptual sketch map shows lithological units and different volcanic outcrop localities (Figure 1, Table) prepared and enhanced with ArcGIS Earth in 2022. Lithological contacts modified after Podjyachev et al. [1, 2], and lava Kildyam Volcanic Complex discovered in the natural outcrops and quarries of the Kangalass terrace in the left bank of the Lena River 26 km north of Yakutsk (ESRI ArcGIS.Imagery after Kostin). Country rock consists of volcanic sequence and intrusive complex represented by magnetite rich lava flows and ultramafic lavas, agglomerate, pyroclastic breccia and tuff of andesites and dacites.

Kildyam iron oxide deposit interpreted as lava flows and feeder dykes formed from iron rich oli-

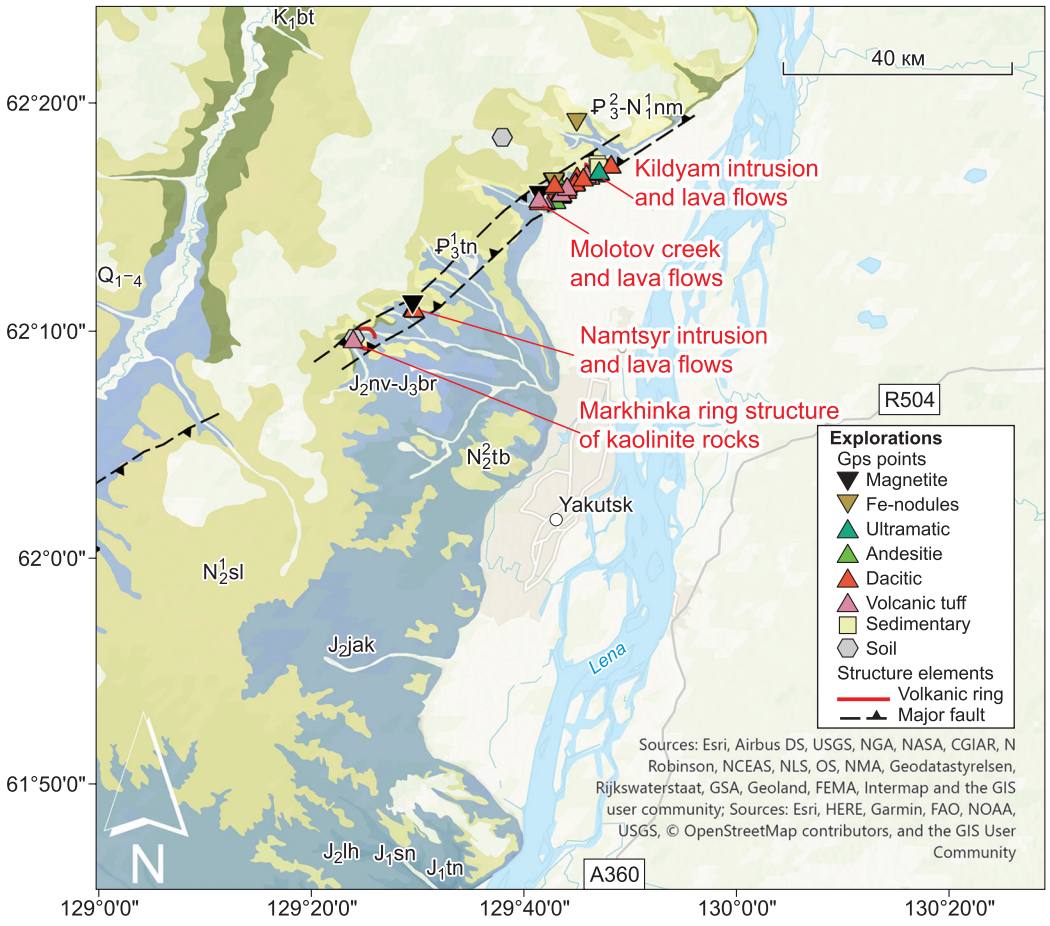

	Q_{1-4}	**Quaternary formation.** Sandy-clay, gravel-pebble (up to 20 m)
	N_2^2tb	**Tabaga formation.** Alluvium of the floodplain terrace of the Lena river. Sands with lenses of gravel and pebble (up to 10 m)
	N_2^1sl	**Solban formation.** Fe-sands, gravel, pebble (20–60 m)
	P_3^2-N_1^1nm	**Nam formation.** Sands, pebbles, aleurites, clays (43 m)
	P_3^1tn	**Tandyn formation.** Sands, aleurites, clays (18 m)
	K_1ex	**Eksenyakh formation.** Coal – free sandstones, widespread development of sideritized sandstone nodules (up to 450 m)
	K_1bt	**Batilykh formation.** Sandstones, siltstones, clays, coals (40–270 m)
	J_2nv-J_3br	**Nijnevilui, markichan and bergein formation.** Undifferentiated sand, siltstones, clays, coals. Ultramafic, andesitic, dactic, melilitic and magnetite lava flows, kaolinite lences (up to 4000 m)
	J_2jak	**Yakut formation.** Sands, sandstones, clays, (60–100 m)
	J_2lh	**Lokhanin formation.** Clays, sandstones, siltstones, (up to 40 m)
	J_1sn	**Suntar formation.** Siltstone, clay, sand (up to 40 m)
	J_1tn	**Tung formation.** Sands, siltstones, clays (80–90 m)
	J_1uk	**Ukugut formation.** Sandstones, siltstones (140–160 m)

Fig. 1. Geological conceptual sketch map showing lithological units and different volcanic outcrop localities; lithological contacts modified after Podjyachev et al. [1, 2]; lava complexes after Kostin. Kildyam framework provide spatial relationship between iron oxide economic emplacement and sulfide Cu, Ag and Au mineralization. *Location and description of the key outcrops in Kildyam lava.* (1) *Kildyam intrusion and lava flows*: Late Jurassic subvolcanic complex of olivine-clinopyroxenite breccia and of iron hydroxides overlie and intrude sedimentary rocks. (2) *Molotov creek and lava flows*: A group of small open pits with red tuff,

mined before 1970 for the roads construction purpose; lava units of 15–20 m thick lie unconformably upon Late Jurassic volcanic sandstone basement. (3) *Namtsyr intrusion and lava flows*: open pit expose a full section from Late Jurassic sandstone, lava, red tuff with flora fossils, coal and sand. These succession lie conformably upon Late Jurassic volcanic sandstone basement; feeder dykes composed of dacitic lava and pumice. (4) *Markhinka ring volcanic structure of kaolinite rocks*; river sections expose cliffs from the riverbed to the top of the annular volcanic plateau. Yellow sand, 0.1 m of coal, and white kaolin clay.

vine-pyroxenite magma because of liquid immiscibility [3]. Associated with andesitic lavas mineralization occur as massive, tabular bodies and stratified pyroclastic ores. Our research confirmed that tholeiitic trend of iron-rich pyroxenites evolves towards two immiscible liquids – magnetite lava and melilitite matrix. Further evolution leads to the separation of native iron and the transition of lavas to the calc-alkaline trend. Immiscibility of iron- and silica-rich melts during andesitic volcanism led to the formation of exotic varieties of magnetite-rich volcanic rocks. Fe–Ti-spinel mineral group is widespread at the Kildyam Volcanic Complex in the host andesite and in the local magnetite ore bodies.

The unique iron-oxide Kildyam melts crystallized in effusive environment with different morphological and structure-textural details. The rapid-growth features attributed to sudden supersaturation due to degassing of oxide melts. Effusive iron-oxide liquids reach the surface via feeder dikes and subparallel swarms of fissures and voids. Main ore product expelled from fissure was a magnetite-rich pyroclastic material, deposited on Kildyam andesitic lavas. Our results of 2017–2021 year research support that occurrences of native copper (Cu), silver (Ag), and gold (Au) in many of magnetite lava flows enriched surface due to vapor transport and imply preconcentration of iron-oxide copper-gold-silver during lava solidification before later hydrothermal remobilization.

Petrographic and microprobe studies confirmed liquid immiscibility in silicate melts during crystallization. Immiscible liquids preserved as globules of one glass in another in andesites and as melted inclusions of native iron in matrix, clinopyroxene and plagioclase phenocrysts. Our analyses reveal the complex textural relationships between silicates and Fe-oxides, native iron and (Cu, Pb, Ag and Au)-rich phases, and provide unequivocal textural evidences, not observed previously. Purpose of this research is to preserve a very important data on IO (Iron Oxide) or IOCG (Iron Oxide Copper Gold) mineralization.

Obtained results support occurrence and diverse of gold, silver, copper and lead minerals in magnetite lavas. During the early stage of fine-grained subvolcanic olivine-clinopyroxenite and pyrrhotite,

Table

Locations and descriptions of the key outcrops of Kildyam lava (updated from 2021 [4])

Locality	Coordinates (dd°mm′ss.s″)	Elevation (m)	Description
(1) 33 km North from Yakutsk, and 1.9 km Northeast towards Nam road direction	62.285375N 129.785478E	141	Kildyam ultramafic intrusion and lava flows. Catalogued in the hillside section exposing subvolcanic complexes; cliffs show signs of mineral accumulation. Small lava flows are common. New discovery with no exploration history
(2) 29 km North from Yakutsk, and 3.5 km West from Kildyam village	62.27425N 129.71313E	160	Molotov creek and lava flows. A group of small open pits with red tuff, mined before 1970 for the roads construction purpose. Lava lying below not mined now, and represent good ground for study. A numerous Late Jurassic flora fossils was collected
(3) 13.5 km North-West from Yakutsk towards Namtsyr road direction	62.18543N 129.493888E	198	Namtsyr intrusion and lava flows. Open pit exposed a full section from Late Jurassic sandstone, lava, and red tuff with flora fossils, coal and sand
(4) A temporary 8.5 km summer road, North-West from Magan airstrip	62.158337N 129.41908E	225	Markhinka ring structure of kaolinite rocks. A new undiscovered volcanic structure. River sections exposing cliffs from the river bed to the top of the annular volcanic plateau

globular igneous sulfides correspond to first proposed style of economic deposit formation. The second stage is of cooking Fe-rich andesitic and K-rich dacitic lavas. The third proposed style of economic mineralization in Kildyam is to be a magnetite-bearing lava; melilitic melt phase, followed by iron depletion and calcium enrichment. Vesicle-hosted alloys and sulfides provide significant new data on metal transport and precipitation from high-temperature magmatic vapors. During syneruptive vapor phase exsolution, volatile metals (Cu–Zn, Fe–Al–Cu, Ni–Fe–Cu–Sn) and Ag–Cu-sulfides contribute to the formation of economic concentrations.

The presence of native iron liquids as melt inclusions in clinopyroxene and plagioclase phenocrysts in andesite matrix, magnetite- and silica-rich globules in olivine-clinopyroxenite matrix, demonstrates the occurrence of liquid immiscibility in the early stage evolution of tholeiitic magmas. Lava flows saturated with native iron, magnetite, troilite and pyrite, native iron usually spherical in shape. According to microprobe analysis native iron contain Co – 0.04–2.89 %; Ni – 0.01–1.09 %; Pt – up to 1.45 %; Ir – up to 2.97 %; Pyrite contain Au – 0.11–2.25 %; Pt – 0.57–2.88 %; Ag – 0–1.18 %; Troilite contain Au – 0–3.15 %; Pt – 0–2.02 %; Ag – 0–1.68 %. In places, the amount of the magnetic fraction reaches 25–30 to 90 % of total of lava flows. In andesitic variolithic lavas the Pt content determined by the ICP-MS method – 0.11 g/t. On the flanks of the volcanic field, alluvial gold known in the Zolotinka stream (Cape Kangalassky) and in Paleogene sediments, discovered by the Khatyng-Yuryakh quarry 8 km from the center of Yakutsk, by A.P. Smelov and A.A .Surnin [5]. Most of the analyzed gold fineness varies from 846 to 996. Among high-fineness gold there is an Ag alloy – electrum that is typical for gold-silver mineralization. Discovered andesite associated iron-oxide ± gold and silver mineralization in Central Yakutia allows referring it to analogous El Laco deposit in High Andes and Kiruna in Sweden [6].

Methods and Analytical Techniques

(1) Initially after Ten-01 volcanic cone discovery and, Kildyam outcrop mapped using an easily identified red tuffs and brecciated flow units. Lava flows traced extensively using satellite maps submitted by ESRI ArcGis.Imagery Service using open geospatial data, software and standards after Bakillah et al., and Minghini et al. [7, 8], interpretation and selective ground reconnaissance in numerous open pits.

(2) All styles of field surface samples classified as volcanic, sedimentary or ore, cut with a circular saw and representative pieces added to the collection. The remaining part of each sample used to prepare polished sections for preliminary mineral identification with polarized light microscopy. Major minerals in lavas and sediments determined by x-ray phase analysis using D2 PHASER diffractometer.

(3) All chemical analyses of volcanic rocks carried out at the Diamond and Precious Metal Geology Institute, Siberian Branch, Russian Academy of Sciences (DPMGI SB RAS). The major oxides compositions analyzed using methods of spectrometry, atomic emission spectrometry, ionometry with ion-selective electrode, gravimetric, titrimetric. The major oxides analyzed SiO_2, TiO_2, Al_2O_3, Fe_2O_3, FeO, MnO, MgO, CaO, Na_2O, K_2O, and P_2O_5. The loss on ignition (LOI) values range from 0 to 0.8%.

(4) Microscopic petrography and microprobe analysis of 120 polished sections conducted to provide detailed data to confirm the phenocrysts and glass chemistry, presence of magnetite and other ore minerals. All microprobe and x-ray analyses carried in the Diamond and Precious Metal Geology Institute, Siberian Branch, Russian Academy of Sciences (DPMGI SB RAS). Samples prepared from polished sections with a sprayed thin conductive layer of carbon. Back-scattered electron (BSE) images and spot analyses of minerals were done using scanning electron microscope JSM-6480LV with energy spectrometer INCA-Energy, accelerating voltage at the cathode 20 kV.

(5) Lava density calculated by weighing in water and by chemical composition of rock. Lower density values of the samples by weighing in water caused by presence of preserved gas component, so final correction carried out according to chemical composition of lava. Measurement results of representative samples (mineral varieties with a density of 3.74–5.1 g/cm^3 belong to ores):

(stage 1) Olivine pyroxenite, sample 1039(1), density 3.41 g/cm^3.

(stage 2.1) Ignimbrite, sample 1044(4), density 2.82 g/cm^3.

(stage 2.2) Variolithic andesite-basalt, sample 1030(4), density 2.92 g/cm^3.

(stage 3.1) Melilitite phase-1 density 3.19 g/cm^3 and melilitite phase-2, sample 1083(2), density 3.74 g/cm^3.

(stage 3.2) Magnetite lava, sample 1042(3), density 5.10 g/cm^3.

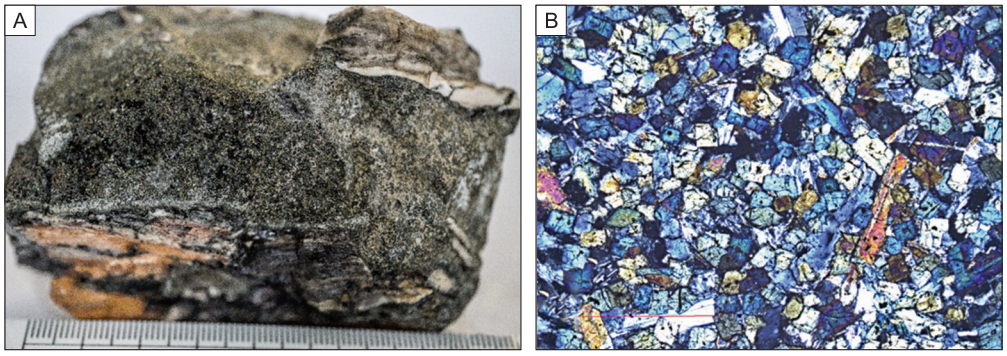

Fig. 2. Ten-01 volcanic cone of dacitic lavas delivers variety of material from great depth. As an example a pyroxenite xenolith in dacitic lava (A) showing a peridotite structure (B). Sample (1019/2) composed (%) of SiO_2 – 37.57, TiO_2 – 0.83, Al_2O_3 – 19.07, Fe_2O_3 – 11.55, FeO – 1.27, MnO – 0.3, MgO – 4.34, CaO – 23.00, Na_2O – 0.32, K_2O – 0.56, H_2O^- – 0.28, H_2O^+ – 0.21, LOI – 0.22, P_2O_5 – 0.03, CO_2 – 0.43, S – 0.03, Total – 99.75.

Massive panidiomorphic granular rock with rare angular interstices filled with plagioclase and carbonate; rock is dominated by large zoned pyroxenes, pyroxenite, sample 1019/2, density 3.11 (Fig. 2). After Kostin [9] magmatic origin of Ten-01 volcano confirmed with mineralization of magnesioferrite, hercynite, fayalite, Al-bearing clinoenstatite, ilmenite, baddeleyite, chromospinelide, and garnets predominated in the products of deep removal of the volcano-anorthosites. After lava solidification, gas-fluid processes along numerous voids connected to each other, and carry Ag, Au, Cu, Ni and increase total value and quality of Fe ore.

Geologic background and lavas collection

Recent studies suggest that immiscible liquids occur in many tholeiitic basalts and some alkaline and calcalkaline lavas [10]. Mantle melting at mid-ocean ridges produces dry magmas that differentiate at low-pressure conditions, resulting in early plagioclase saturation, late oxide precipitation, and Fe-enrichment [11]. Representative collection of immiscible liquids preserved as chemically distinct, glassy globules [12], Si-rich and Fe-rich samples of Kildyam pyroclastic rocks and associated mineralization grouped into succession of 5 stages. (**1**) Olivine-clinopyroxenite with sulfide liquid globules [13]: alloys – $Au_{(Ag,Cu,Fe)}$; sulfides – troilite, pyrrhotite, chalcopyrite, argentite. (**2**) Andesitic lava with large segregations and drops of native iron [14]: alloys – native iron; sulfides – $pyrrhotite_{(Co,Ni,Cu)}$. (**3**) K-rich dacitic and rhyolithic glass, and vesicles [15] of heavy sulfide minerals: sulfides – pyrite and bartonite. (**4**) Olivine-(fayalite) melilitites are ultrabasic, ultramafic, volcanic rocks [16] characterized by high concentration of CaO and FeO, and relatively low Al_2O_3. Melilitic lava [16] with globular disseminated chalcopyrite: sulfides/sulfates – chalcopyrite and barite. (**5**) Lava of fused magnetite crystals [17] and voids with alloys [18] and sulfides: oxides – magnetite; alloys – Au, Cu–Fe–Ni–Sn, Fe–Co–Ni–Cu, Cu–Al–Mn; sulfides – argentite, galena, chalcopyrite, tetrahedrite and arsenopyrite [19].

Olivine-clinopyroxenite include 48.1 % of pyroxene (augite, rarely hedenbergite), 23.6 % of plagioclase (bitownite-anorthite), 16.8 % of olivine (average $Fo_{0.105}Fa_{0.895}$), 6.07 % of magnetite, 1.79 % of calcite and 0.75 % of troilite. Less common minerals are Ba-feldspar celsian and K–Ba-feldspar hyalophane. Ore minerals concentrated in up to 1.0 cm in size globules, surrounded by olivine rims. Pyroxenite is heavy (3.41 g/cm^3), fine-grained black rock of allotriomorphic and rarely panidiomorphic structure with FeO_{total} content > 32 %. Ore globules composed of magnetite and troilite in equal proportions. According to Craig and Kullerud troilite, pyrrhotite, chalcopyrite, and ± pentlandite is a typical sulfide assemblage from mafic magmas. Segregations of subspherical agglomerations interpreted as sulfide liquids; in places form elongated clusters up to 3 cm in length. Globules as sulfide phases in Kildyam olivine-clinopyroxenite melt (about 89-mol % of Fa) completely filled with sulfides and consisting mainly of pyrrhotite and less often troilite (Fig. 3).

Variolithic lavas are widely distributed in Kildyam andesite succession Figure 4. Silicate and iron immiscibility indicated by occurrence of varioles (globules) with different chemical composition and different matrix. Outcrops showing that andesitic lavas first penetrate as feeder dikes through Late Jurassic sandstones (3.0 m) along a fissure conduit and then cover the sandstones with 2–5 m layer [20]. Lava flow covered with a layer of crystalloclastic

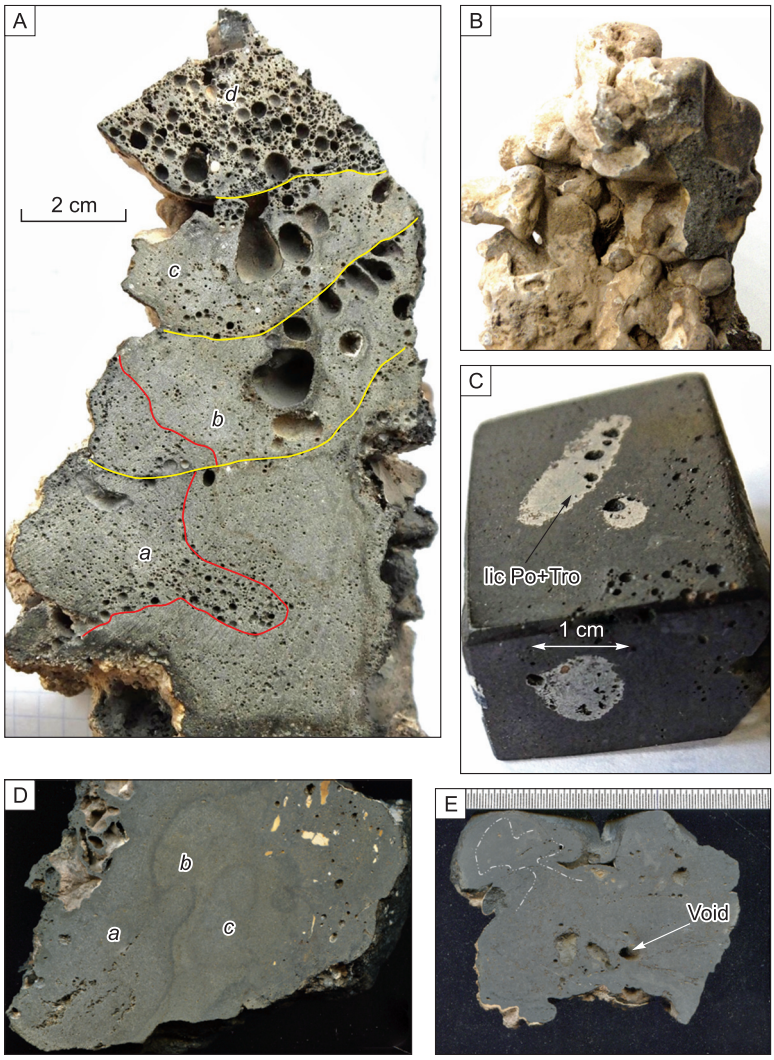

Fig. 3. This unit includes two different deposits styles (a lot of vesicle at 184 m and a little at 99 m) derived from subvolcanic complex overlie and intrude Late Jurassic sedimentary rocks. A – Multistage carapace lavas of down-flow textural modifications, sample 1051 (location 62.285457° 129.786033° 184 m) with (*a*) – flow fold; (*b*) – lava layer shift; (*c*) – degassing channel; (*d*) – another degassing channel with extra porous. Coalescence of vesicles may produce 10–20 cm-sized vesicles or lava blisters there – and a zone of pipe vesicles along the base. B – Morphologies of a lava flow unit comprising massive olivine-clinopyroxenite small lava flows, autobreccias, and scoria deposits, derived from small scoria and lava flows. C – Polished olivine-clinopyroxenite sample with immiscible sulphide globule and tube segregations of elongated morphology, sample 1039 (location 62.284879° 129.786620° 99 m [4]). D – Flow textures characterize morphologies of a lava flow, identify lava flow border features, and provide insight into eruption conditions. E – Individual flow-unit vary from 2 cm to 10 cm thick; typical features are a concentration of vesicles in the uppermost unit. Abbreviations: licPo+Tro Pyrrohotite liquid immiscible texture, lic Tro – Trolite immiscible texture.

tuffs, about 1.5 m thick, and brecciated by the next andesite lava flows. Kildyam andesites contain inclusions of black graphitized coal up to 2–2.5 mm in size with no signs of burning. The brand of the lamellae of clinopyroxene and plagioclase in contact with coal wrap around these inclusions. Lavabreccias represented by various-sized fragments of hyalopilite andesites or variolithic andesibsalts in bubble glass of hyaline structure of dacite-rhyodacite composition, containing the smallest microliths, comminuted grains and feldspar crystallites. Clastolava include large pyroxenite xenoliths, were grains of partially uralized clinopyroxene germinate with andesite plagioclase leists.

Several small dacitic extrusive cones and scoria forms silicic eruptive sequence. Volcanic cone of about 180 m (location 62.263333° 129.692529°) exposed within small open pit, on the edges structure represented by extrusive dome and volcanic breccias, accumulations of pumice and scoria.

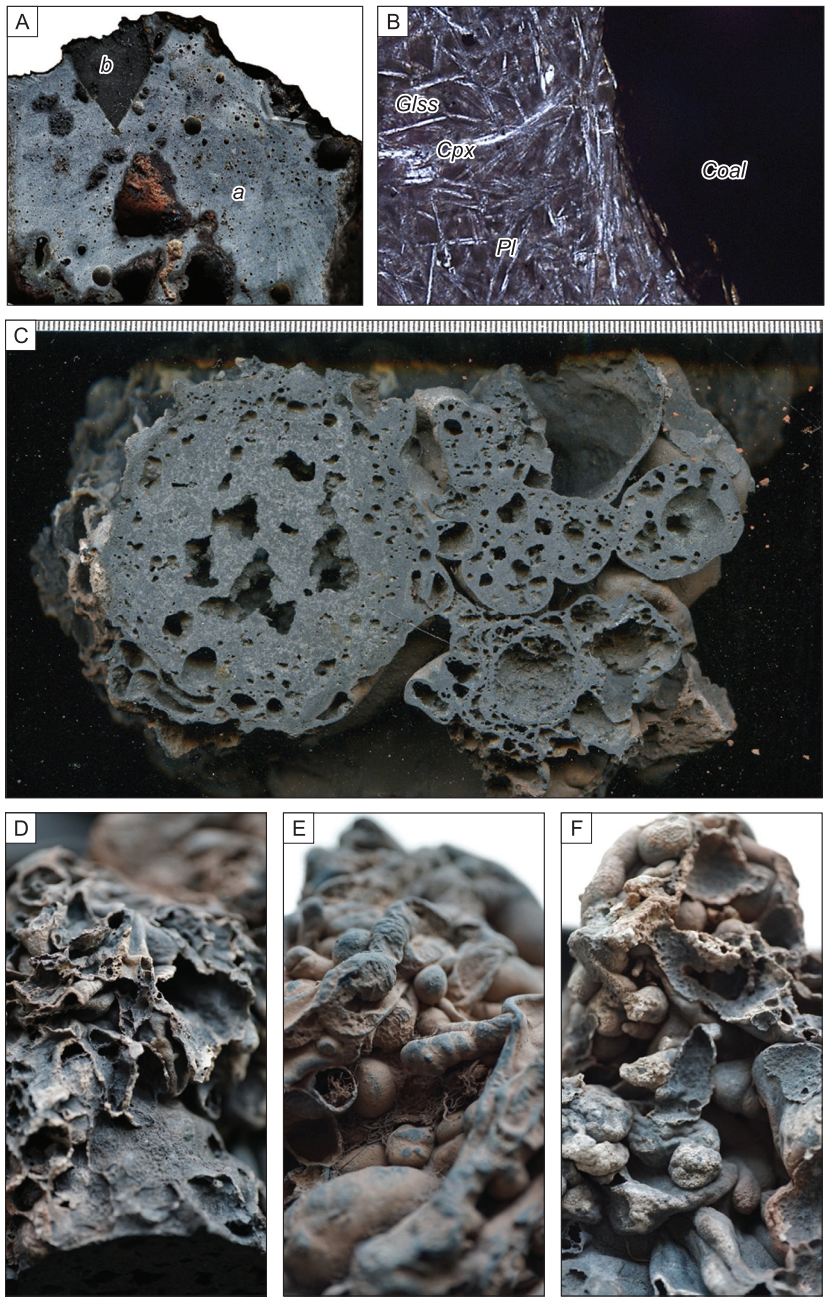

Fig. 4. Diverse variolithic andesitic lavas. A – Bubbling variolithic andesite lava with coal fragments, sample 1030/4 (location 62.26892 129.72371 141 m [20]). B – Variolithic basalt-andesite in contact with a fragment of graphitized coal (section 1030/4, magnification 100, nicol ×) composed of radially radiant intergrowths of clinopyroxene, plagioclase and glass. C – This unit groups basaltic andesite small volcanoes and isolated scoria and lava cones, sample 1066 (location 62.26952 129.72657 143 m). D–F – Examples of lava flows lobes indicate flow direction; lava lobe formed by numerous vesiculated carapace. One small unit has clearly emerged from a crack (arrowed) in the crust of another unit. Porphyritic compound flows often show striking variations content attributed to gravity settling, not only between one flow-unit and another but also between top and bottom of the same unit. Abbreviations: Glss – Glass, Coal – Coal, Cpx – Clinopyroxene, Pl – Plagioclase.

Sandstone fragments cemented by lava flow, indicating that lava penetrated under the flow. Lava-breccias represented by fragments of anneal sandstone displaced and cemented with lava flow, composed of glass, banded lavas, lava breccias, pumice stones, and carapase. Dacites protruding viscous lava and forms a column about 4 m high above the cone and bending of the dacitic lava flow from a feeder channel, extrusive volcanic cone with lava flow texture streaming rises up the vent and then

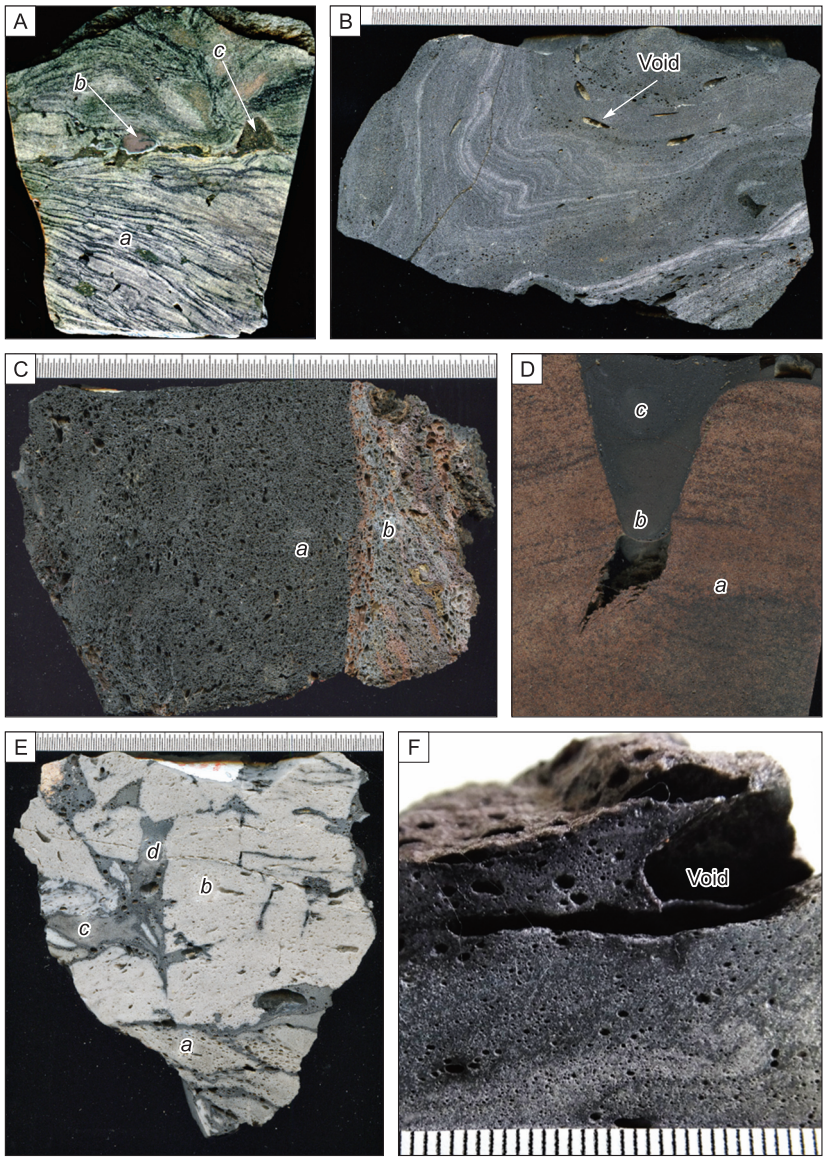

Fig. 5. This ignimbrite records caldera-forming eruption of dacitic and riodacitic lava and red tuff exposing in the upper volcanic zone. A – Riodacite ignimbrites, sample 1044/3 (location 62.263997° 129.716967° 149 m) introduced with light fragments of cristaloclastic porous lava and black elongated scraps and lenses of glass. On the ignimbrite border scraps of a fayalite–bytownite–hedenbergite (*a*) and fayalite–hercynite–hematite (*b*) from subvolcanic complex [20]. B – Volcanic flow composed of glass, banded lavas, lava breccias, pumice stones, and carapase, elongated scraps and lenses of glass; wavy lava, sample 1033/5 (location 62,27024 129,71787 140 m) were light – lava with crystallites, dark – obsidian. C – Black (*a*) and reddish (*b*) pumice, sample 1050/1 (location 62.18487 129.4961 199 m). D – Crack in crystalloclastic tuffs (*a*) filled with lava crystalloclastic tuffs (*b*) and lavabreccias (*c*), sample 1055 (location 62.2635 129.70134 151 m). Volcanic structure represented by an extrusive dome and volcanic breccias on the edges, accumulations of pumice and scoria [20]. E – Lavabreccias represented by fragments of anneal sandstone (*a*) displaced and cemented with lava flow; brecciated lava (*b*) and (*c*) with crystallites, dark – obsidian cement (*d*), sample 1049 (location 62.18565 129.4937 194 m). F – Bubble textures of lava flows suggest style of solidification were lava moving along the slope, and shape of bubbles usually elongated, sample 1033/5 (location 62.27024 129.71787 140 m) [20].

falls on its side. Dacitic lava unpredictably penetrate as small domes, composing extrusive cones. Investigated lava represent examples of different flow facies, as defined by A.V. Kostin and V.A. Trunilina [21] in the flow emplacement mechanisms. Ash red tuffs contain fragments of uncrystallized glass, crystals and their angular fragments. In some cases, dark bands represented by obsidian, in others – by bubbly to-foamy rhyodacite with larger void sizes than in the light bands and the predominance of the vitreous hyalopylite matrix over the crystalline phase (Fig. 5).

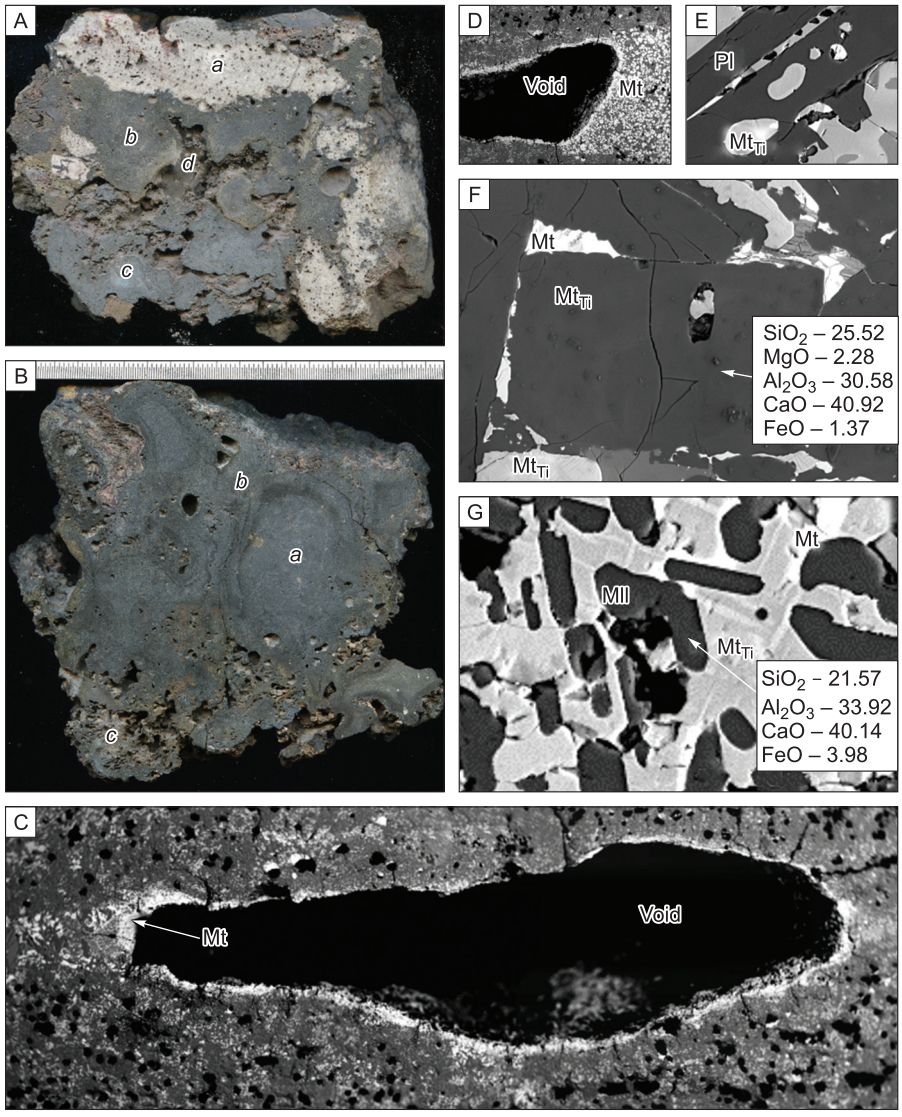

Fig. 6. A – Lavabreccias represented by fragments of anneal sandstone (*a*) displaced and cemented with lava flow (*b*); (*c*) melilitic lava-breccia and (*d*) voids, sample 1049 (location 62.18565 129.4937 194 m). B – Melilitite lava with spherical texture and minor sulfides: (*a*) SiO_2 – 37.32, MgO – 2.47, Al_2O_3 – 16.90, K_2O – 0.85, CaO – 22.12, FeO_{tot} – 19.60, Total 99.26 [sample 1083-2/1(3)]. (*b*) SiO_2 – 11.92, MgO – 3.74, Al_2O_3 – 16.35, CaO – 20.67, FeO_{tot} – 47.42, Total 100.10 [sample 1083-2/13(4)]. (*c*) – Voids. C–G – *Back-scattered electron images of representative melilitic lavas*. C – Elongated shape of voids show flow-units and lava movment; framing of magnetite [sample 1071-12/12(2)]. D – Magnetite accumulating in shadow of degassing voids: SiO_2 – 39.85, TiO_2 – 2.38, Al_2O_3 – 11.70, CaO – 1.73, FeO_{tot} – 43.63, Total – 99.30 [sample 1071-12/25(4)]. E – Structure of magnetite immiscibility: MgO – 15.95, MnO – 3.34, CaO – 1.16, FeO_{tot} – 80.37, Total – 100.83 [1083-01/18(5)] and melilite: SiO_2 – 21.72; Al_2O_3 – 33.02; CaO – 39.47; FeO_{tot} – 3.94, Total – 98.14 [sample 1083-01/18(10)]. F – Melilite (prevail) SiO_2 – 21,57; Al_2O_3 – 33,92; CaO – 40,14; FeO_{tot} – 3,98; Total – 99,61 [sample 1083-02/14(4)] – magnetite MgO – 16,81; MnO – 2,80; FeO_{tot} – 80,06; Total – 99,67 [sample 1083-02/14(10)] intergrowth. G – Melilite SiO_2 – 21,57; Al_2O_3 – 33,92; CaO – 40,14; FeO_{tot} – 3,98; Total – 99,61 [sample 1083-02/14(4)] – magnetite (prevail) MgO – 16,81; MnO – 2,80; FeO_{tot} – 80,06; Total – 99,67 [sample 1083-02/14(10)] intergrowth. Abbreviations: Mll – Melilite, Mt – magnetite, Mt_{Ti} – Ti-magnetite, Pl – Plagioclase, Void – Void.

Melilitic lavas assemblage is made up of melilite mineral group – Fe-akermanite $Ca_2(Mg,Fe^{2+})(Si_2O_7)$ (prevail) + clinopyroxene + feldspathoids + hyalophane or celsian [22]. According to the bulk composition (in %): SiO_2 – 36.32, TiO_2 – 0.62, Al_2O_3 – 11.83, Fe_2O_3 – 16.99, FeO – 4.47, MnO – 0.66, MgO – 1.95, CaO – 17.08, Na_2O – 0.54, K_2O – 1.16, H_2O^- – 1.21, H_2O^+ – 1.8, LOI – 2.14, P_2O_5 – 0.03, CO_2 – 1.62, S – 1.55 lava corresponds to melilititic and melilite-bearing volcanic rock Fig. 6.

Magnetite ore bodies with the general form of lava flows exposed on flanks of El Laco volcano in the central Andes [23]. Many small-scale features observed at Kildyam very closely resemble textures formed from direct solidification of magmas. Magnetite lava showing immiscibility of iron- and silica-rich melts during andesitic volcanism led to the formation of exotic varieties of magnetite-rich volcanic rocks. Fe–Ti-spinel minerals group is widespread at the Kildyam Volcanic Complex in the host andesite and in local magnetite ore bodies. Iron-rich lava identified as two main types – rich titaniferous magnetite iron ore and magnetite lava, containing magnetic fraction from 25 to 37 % of total volume (Fig. 7). Magnetite-rich lava identified as titaniferous magnetite iron ore, containing magnetic fraction from 25 to 37 % of total volume and magnetite lava. All magnetite crystals trapped in the silicate matrix, composed (in %) of: SiO_2 – 35.5, TiO_2 – 0.9, Al_2O_3 – 7.5, FeO_{total} – 13.96, MgO – 3.91, CaO – 37.38, Na_2O – 0.45, K_2O – 0.75. Petrographic and microprobe studies confirmed the immiscible liquids as Fe–Ti-spinel minerals group, local magnetite ore bodies. This type of magnetite comprises that of the main massive magnetite mineralization at Kildyam. In magnetite-rich lavas FeO_{tot} content reach 70.8 % and ultra-rich magnetite lava contain 94.08 % of FeO_{tot}. Many small-scale, features observed at El Laco [24] and at Kildyam [4, 25] very closely resemble textures formed from the direct solidification of magmas.

Kildyam rock succession

To guide future research, this study investigate geological evolution and the emplacement of the Kildyam complex of andesites, rhyodacites and intrusive/extrusive ultramafic and magnetite-rich bodies constitute Yakut Formation. Kildyam representative sampling program built upon the work of 2017–2021 wherein the intact portion of 17 small open pit ever described.

Kildyam occur as massive, sub horizontal tabular bodies, crosscutting fider dikes, and as stratified fragmental material lava flows. Major conclusions contribute to 3-step genetic model. (1) Early-formed magmatic minerals led to partial dissolution of olivine-clinopyroxenite and their enrichment in Cu, Co and Ni relative to other metals, when troilite globules droplets grew. (2) First stage of division into two immiscible silicate and sulfide melt liquids; (*a*) K-rich dacitic and rhyolithic glass, and (*b*) vesicles of heavy sulfide minerals with a large segregations and drops of native iron. (3) Globular disseminated chalcopyrite in mineralized melilitic rocks (a), and lava of fused magnetite crystals and voids enriched in silver and gold (b).

Sulfide mineral and bulk rock compositions determined from samples in olivine-clinopyroxite, andesite, dacite, melilitite, and magnetite lavas, sulfides high in Ni, and Co (troilite, pyrrhotite, chalcopyrite, pyrite, and bartonite), and metals (iron, copper, gold, and silver). Platinum-group element (PGE) compositions also determined for two samples (0.11 ppm) ICP MS. Numerous silicate, Fe-oxide, and Cu microspherules found in Fe ores and pyroclastic rocks, silicate spherules contain immiscible Fe and Si glasses, vapor voids, and mineral inclusions. Fe-oxide spherules host magnetite with a small amount of ilmenite and Fe-rich silicate glass.

Low S content in Kildyam magma come initially from fayalite, clinopyroxene, plagioclase and magnetite parent magma. All Kildyam volcanic processes somehow occur in connection with iron enrichment. During the early stage of fine-grained subvolcanic olivine-clinopyroxenite end pyrrhotite; globular igneous sulfides is a first proposed style of economic deposit formation. Second proposed style of economic mineralization in Kildyam is to be a magnetite-bearing lava; iron enrichment of the melilitic melt phase, followed by iron depletion and silica enrichment. Kildyam magnetite crystallization mark the end of absolute iron enrichment in magma. Early Jakobsen et al., documented immiscible iron-and silica-rich melts in the Skaergaard intrusion [27] as a similar example in Kildyam [4]. Accumulation of large sulfide volumes, fayalite and augite near the surface, indicate possible existence of substantially heavier rocks located deeper. This is confirmed with a presence of an unusual complicated mineral phase of spinelide, discovered in andesite-variolitic lavas; it is a mix of ulvespinel (Fe_2TiO_4) ± spinel ($MgAl_2O_4$), enriched with Nb. Back-scattered electron image show fragments of ulvespinele skeletal crystal in glass matrix, which most likely came from olivine-clinopyroxenite.

The vesicle-hosted alloys and sulfides provide significant new data on metal transport and precipitation from high-temperature magmatic vapors. During syneruptive vapor phase exsolution volatile metals (Cu–Zn, Fe–Al–Cu, Ni–Fe–Cu–Sn) and Ag–Cu-sulfides contribute to the formation of economic concentrations. Our research confirmed that tholeiitic trend of iron-rich olivine-pyroxenites evolves

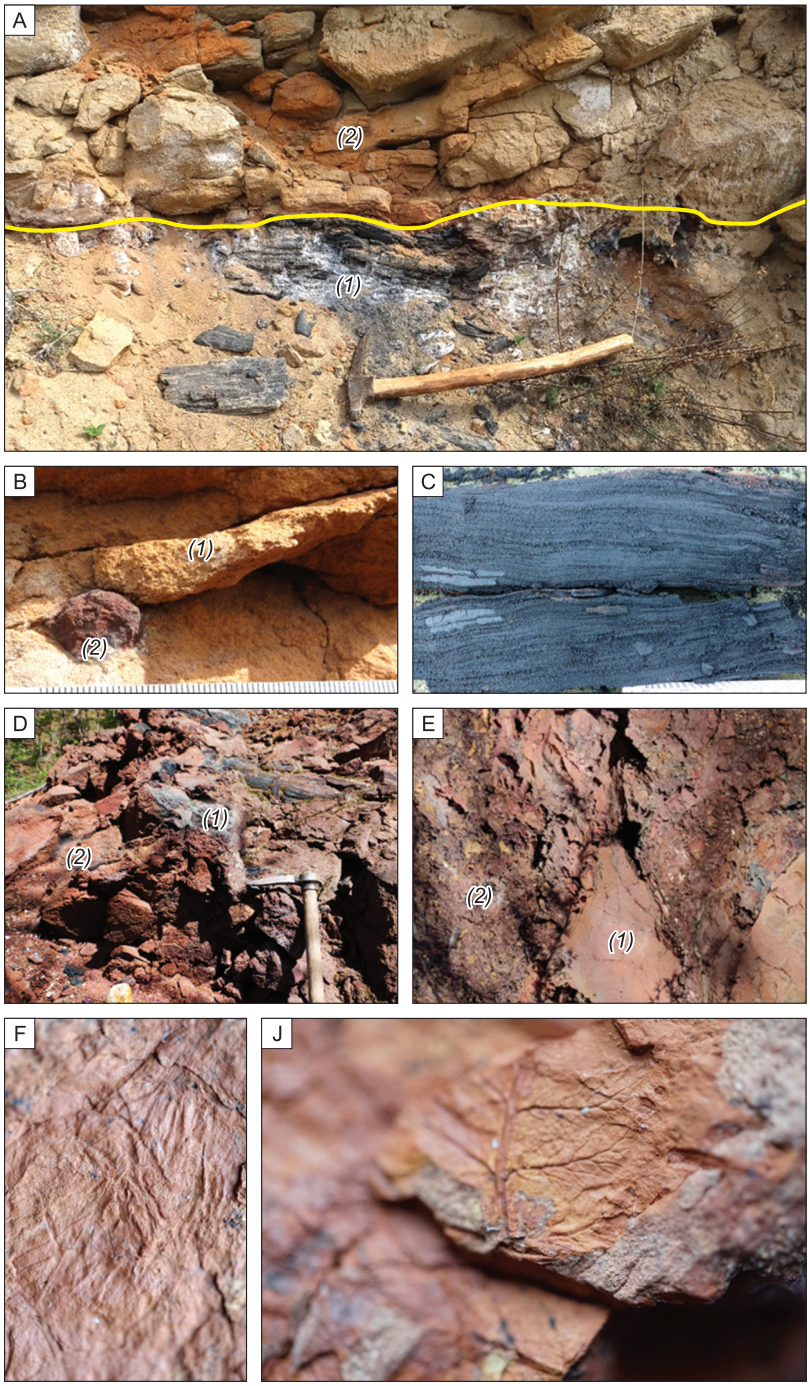

Fig. 7. Field photographs from the outcrop of volcanic formation in Kildyam Volcanic Complex (left side of the Lena River) and rock samples (sample1068-2020.png; 129.735714° 62.27391° 134 m). A – Magnetite lava with contorted flow structure (*1*) and overlying units of pyroclastic tuff-sandstone (*2*). B – Sheeted structure of pyroclastic reddish-yellow tuff-sandstone and lapilli spheroids of magnetite crystals in Fe-hydroxide cover. **C** – This photograph is a close-up of the outcrop depicted in magnetite lava with well-developed sheeted structure due to laminar flow and close up of a magnetite plate in skeleton ore showing parallel growth. D – The basal part of the flow units frequently developed as a series of 2- to 10-cm-thick dense sheets with distinct surfaces of separation (sample1068-2020.png; 129.735714° 62.27391° 134 m). Fragments of magnetite lava filling red tuff. E – Lava flow brecciating a layer of crystalloclastic tuff with thin magnetite lava flows. F–J – Red and reddish-brown crystalloclastic volcanic tuff of Upper Jurassic flora contain fossils of leaf flora typical of Bergeya Formation in Aldan River basin; age of leaf flora determined as Late Jurassic by A. Kirichkova in St. Petersburg, VNIGRI Fern of *cladophlebis C*. cf. *aldanenis* Vachrameev; *Nilssonia* [26].

towards two immiscible liquids – magnetite lava and melilitite matrix. Further evolution lead to the separation of native iron and the transition of lavas to the silica-rich calc-alkaline trend. Petrographic and microprobe studies confirmed the liquid immiscibility in silicate melts during crystallization [28]. Immiscible liquids are preserved as globules of one glass in another in andesites and as melted inclusions of native iron in matrix, clinopyroxene and plagioclase phenocrysts.

Major conclusions contribute to three-step genetic model. (*1*) Early-formed magmatic minerals led to partial dissolution of olivine-clinopyroxenite and their enrichment in Cu, Co and Ni relative to other metals, while troilite globules droplets grew. (*2*) Second stage of division into two immiscible silicate and sulfide melt liquids (a) K-rich dacitic and rhyolithic glass, and (b) vesicles of heavy sulfide minerals with a large segregation and drops of native iron. (*3*) Third stage (a) lava of fused magnetite crystals and voids enriched in silver and gold, and (b) globular disseminated chalcopyrite in mineralized melilitic rocks. A chemical classification of Kildyam volcanic rocks based on the total alkali-silica diagram Fig. 8.

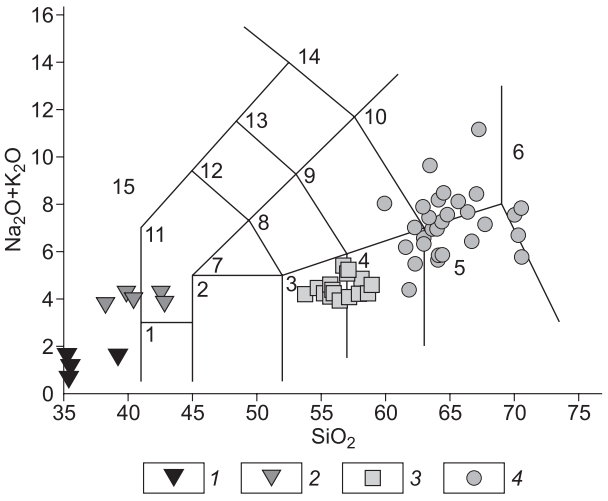

Fig. 8. SiO_2 – K_2O+Na_2O TAS diagram after LeBas, et al. [29], and variation diagram showing trend defined by composition of Kildyam volcanic rocks associated with iron-rich mineralization: *1* – olivine-pyroxenite, *2* – melilitite matrix in magnetite lava, *3* – andesitic, *4* – dacitic. Low-silica intervals composed of magnetite lavas and are off TAS diagram limits (from 34 to 5 wt % of bulk).
Areas on the graph: 1 – Picrobasalt, 2 – Basalt, 3 – Basaltic andesite, 4 – Andesite, 5 – Dacite, 6 – Rhyolite, 7 – Trachybasalt, 8 – Basaltic trachyandesite, 9 – Trachyandesite, 10 – Trachyte-trachydacite, 11 – Tephrite Basanite, 12 – Phonotephrite, 13 – Tephriphonolite, 14 – Phonolite, 15 – Foidite.

Conclusion

This contribution presents the first detailed compilation of a new volcanic succession (see Fig. 1) of olivine-pyroxenite, andesite, dacite, melilitite and magnetite lavas discovered in the Kildyam that constitute a new iron oxide-(±Cu, Ag, Au) deposit in the Late Jurassic volcanic complex in Central Yakutia.

Effusive iron oxide melts reach surface of J_3br Upper Jurassic Bergeinsky suite (undifferentiated sands, siltstones, clays, coals). Ultramafic (see Fig. 3), andesitic (see Fig. 4), dacitic (see Fig. 5), melilitic (Fig. 6), and magnetite lava (see Fig. 7) flows penetrate across feeder dikes, subparallel fracture, and void swarms. The main ore product coming from the cracks is a magnetite-rich pyroclastic material deposited on andesitic and dacitic lavas. Heavy magnetite lava (rock density 5.1 g/cm^3) characterized by textures:

(a) Rounded fragments of altered volcanic rocks in a magnetite matrix;

(b) Ascending transition from dense magnetite lava to strongly bubbly lava;

(c) Pyroclastic ore dominated by lapilli-sized material;

(d) Magnetite lava with a well-developed layered structure due to laminar flow;

(e) Magnetite volcanic lava from the top of stream;

(f) Lens stratification of pyroclastic ore in a magnetite lava flow.

Final ore product of volcanic process consists of magnetite, less hematite, pyroxene, and rarely apatite. Mining at Kildyam show that most of ore is loose and resembles pyroclastic material; hard ore occurs subordinately. Loose ore is a porous filler of 0.2–1.0 mm magnetite octahedrons with local stratification determined by thin layers of voids of mm. Stratiform Fe-oxide–Cu–Au mineralization within Kildyam Complex is representative. Formation of massive iron deposits linked to many explosive volcanic eruptions, from Ovalle et al. [30], mineralization caused by high oxide and low sulphur saturation, delineated multi-element iron, titanium, copper, gold, and silver occurrence. Corriveau [31] reveal that Iron oxide copper-gold deposits are of worldwide perspective. This new expedition extended investigation area into the nature of the volcanic events in the Kildyam volcanic succession in Central Yakutia. Based on research carried out so far, it is generally accepted that Kildyam group have potential to become world-class size IOCG deposit at 30 km near Yakutsk.

References

1. *Podjyachev B.P., Prokopiev V.S., Andreev A.P., Nikolaeva L.S.* YNV. State geological map of the Russian Federation on a scale of 1:200 000 with an explanatory note. Nizhneamginskaya series. Sheet P-52-XVI (Yakutsk). St. Petersburg, 2004.

2. *Podjyachev B.P., Prokopiev V.S., Andreev A.P., Nikolaeva L.S.* YNV. State geological map of the Russian Federation on a scale of 1:200 000 with an explanatory note. Nizhneamginskaya series. Sheet P-52-XXII (Pokrovsk). St. Petersburg, 2004.

3. *Sillitoe R.H., Burrows D.R.* New field evidence bearing on the origin of the El Laco magnetite deposit, northern Chile // Econ. Geol. [Internet]. 2002. Aug 1. No. 97(5). P. 1101–1109. Available from: https://doi.org/10.2113/gsecongeo.97.5.1101

4. *Kostin A.V.* Mineralization in the Kildyam mafic volcanic rocks-a magmatic contribution to ore-forming fluids (Central Yakutia, Russia) // Arct. Subarct. Nat. Resour. [Internet]. 2021. Vol. 26(2). P. 49–71. Available from: https://doi.org/10.31242/2618-9712-2021-26-2-3

5. *Smelov A.P., Surnin A.A.* Gold of the city of Yakutsk // Sci First Hand [Internet]. 2010, No.4 (34). P. 16–19. Available from: https://cyberleninka.ru/article/n/zoloto-goroda-yakutska

6. *Nystroem J.O., Henriquez F.* Magmatic features of iron ores of the Kiruna type in Chile and Sweden; ore textures and magnetite geochemistry // Econ Geol [Internet]. 1994. Jul 1. No. 89(4). P. 820–839. Available from: https://doi.org/10.2113/gsecongeo.89.4.820

7. *Minghini M., Mobasheri A., Rautenbach V., Brovelli M.A.* Geospatial openness: from software to standards & data. Open Geospatial Data // Softw Stand [Internet]. 2020. No. 5(1). P. 1. Available from: https://doi.org/10.1186/s40965-020-0074-y

8. *Bakillah M., Liang S.* Open geospatial data, software and standards. Open Geospatial Data, Softw Stand [Internet]. 2016. No. 1(1). P. 1. Available from: https://doi.org/10.1186/s40965-016-0004-1

9. *Kostin A.V.* Mineral parageneses of the anorthositic xenoliths and ore potential of the upper Cretaceous volcano «Shadow-01» (Lena-Vilyuy region, East of the Siberian platform) // Arct. Subarct. Nat. Resour. [Internet]. 2015. No. 2(78). P. 35–41. Available from: https://elibrary.ru/item.asp?id=25981696

10. *Philpotts A.R.* Compositions of immiscible liquids in volcanic rocks // Contrib to Mineral Petrol [Internet]. 1982. Vol. 80(3). P. 201–218. Available from: https://doi.org/10.1007/BF00371350

11. *Chin E.J., Shimizu K., Bybee G.M., Erdman M.E.* On the development of the calc-alkaline and tholeiitic magma series: A deep crustal cumulate perspective // Earth Planet. Sci. Lett. [Internet]. 2018. No. 482. P. 277–287. Available from: https://www.sciencedirect.com/science/article/pii/S0012821X17306520

12. *Keller T., Hanchar J.M., Tornos F., Suckale J.* Formation of the El Laco magmatic magnetite deposits by Fe-Si melt immiscibility and bubbly suspension flow along volcano tectonic faults // AGU Fall Meeting Abstracts. 2018. P. V43H–0231.

13. *Hunter E.A.O., Hunter J.R., Zajacz Z., Keith J.D., Hann N.L., Christiansen E.H., et al.* Vapor transport and deposition of Cu-Sn-Co-Ag alloys in vesicles in mafic volcanic rocks // Econ. Geol. [Internet]. 2020. Vol. 115(2). P. 279–301. Available from: https://doi.org/10.5382/econgeo.4702

14. *Andersen J.C.* Postmagmatic sulphur loss in the Skaergaard intrusion: implications for the formation of the Platinova Reef // Lithos [Internet]. 2006. Vol. 92(1–2). P. 198–221. Available from: https://doi.org/10.1016/j.lithos.2006.03.033

15. *Polacci M., Corsaro R.A., Andronico D.* Coupled textural and compositional characterization of basaltic scoria: Insights into the transition from Strombolian to fire fountain activity at Mount Etna, Italy // Geology [Internet]. 2006 Mar 1. Vol. 34(3). P. 201–204. Available from: https://doi.org/10.1130/G22318.1

16. *Minissale S., Zanetti A., Tedesco D., Morra V., Melluso L.* The petrology and geochemistry of Nyiragongo lavas of 2002, 2016, 1977 and 2017 AD, and the trace element partitioning between melilitite glass and melilite, nepheline, leucite, clinopyroxene, apatite, olivine and Fe-Ti oxides: a unique scenario // Lithos. [Internet]. 2019. Vol. 332–333. P. 296–311. Available from: https://www.sciencedirect.com/science/article/pii/S0024493719300933

17. *Andersson J.B.H., Bauer T.E., Martinsson O.* Structural evolution of the Central Kiruna Area, Northern Norrbotten, Sweden: Implications on the geologic setting generating iron oxide-apatite and epigenetic iron and copper sulfides // Econ. Geol. [Internet]. 2021 Dec 1. Vol. 116(8). P. 1981–2009. Available from: https://doi.org/10.5382/econgeo.4844

18. *Godel B., Rudashevsky N.S., Nielsen T.F.D., Barnes S.J., Rudashevsky V.N.* New constraints on the origin of the Skaergaard intrusion Cu–Pd–Au mineralization: Insights from high-resolution X-ray computed tomography // Lithos [Internet]. 2014. Vol. 190–191. P. 27–36. Available from: https://www.sciencedirect.com/science/article/pii/S0024493713004027

19. *Kamenetsky V.S., Belousov A., Sharygin V.V., Zhitova L.M., Ehrig K., Zelenski M.E., et al.* High-temperature gold-copper extraction with chloride flux in lava tubes of Tolbachik volcano (Kamchatka) // Terra Nov [Internet]. 2019. Dec. Vol. 31(6). P. 511–517. Available from: https://doi.org/10.1111/ter.12420

20. *Kostin A.V.* Immiscible silica- and iron-rich melts at the Kildyam volcano complex (central Yakutia, Russia) // Arct. Subarct. Nat. Resour. [Internet]. 2020. Vol. 25(2). P. 25–44. Available from: https://doi.org/10.31242/2618-9712-2020-25-2-2

21. *Kostin A.V., Trunilina V.A.* Volcanogenic creations of Kangalassky terrace (left bank of the Lena River, Central Yakutia) // Adv. Curr. Nat. Sci. [Internet]. 2018.

No. 5. P. 92–100. Available from: https://doi.org/10.17513/use.36761

22. *Melluso L., Morra V., Gennaro R.* de'. Coexisting Ba-feldspar and melilite in a melafoidite lava at Mt. Vulture, Italy: Role of volatiles and alkaline earths in bridging a petrological incompatibility // Can. Mineral [Internet]. 2011. Aug. 1. Vol. 49(4). P. 983–1000. Available from: https://doi.org/10.3749/canmin.49.4.983

23. *Henríquez F., Naslund H.R., Nyström J.O., Naranjo J.A.* Igneous textures in magnetite eruptive products at El Laco, Chile // Int. Assoc. Volcanol. Chem. Earth's Inter. (IAVCEI). Gen. Assem. (abstract poster). Pucón-Chile, 2004.

24. *Soldati A., Farrell J.A., Wysocki R., Karson J.A.* Imagining and constraining ferrovolcanic eruptions and landscapes through large-scale experiments // Nat. Commun. [Internet]. 2021. Vol. 12(1). P. 1711. Available from: https://doi.org/10.1038/s41467-021-21582-w

25. *Kostin A.* Mineralization in the andesitic lava from Kildyam volcanic complex, central Yakutia, Russia // IOP Conf. Ser. Earth Environ. Sci. [Internet]. 2021. Vol. 906(1). P. 12006. Available from: http://dx.doi.org/10.1088/1755-1315/906/1/012006

26. *Grinenko V.S., Kostin A.V., Kirichkova A.I.* New data on the upper jurassic – lower cretaceous rocks in the Eastern Siberian platform // Vestn. Vor. Gos. Univ. Ser. Geol. [Internet]. 2018. No. 2. P. 48–55. Available from: http://doi.org/10.18411/vgu-sg-2018-2-48-55

27. *Jakobsen J.K., Veksler I.V., Tegner C., Brooks C.K.* Immiscible iron-and silica-rich melts in basalt petrogenesis documented in the Skaergaard intrusion // Geology [Internet]. 2005. Vol. 33(11). P. 885–888. Available from: https://doi.org/10.1007/s00410-009-0416-3

28. *Lledo H.L., Naslund H.R., Jenkins D.M.* Experiments on phosphate–silicate liquid immiscibility with potential links to iron oxide apatite and nelsonite deposits // Contrib. to Mineral. Petrol. [Internet]. 2020. Vol. 175(12). P. 111. Available from: https://doi.org/10.1007/s00410-020-01751-8

29. Bas M.J.L.E., Maitre R.W.L.E.*, Streckeisen A, Zanettin B.* Rocks IS on the S of I. A chemical classification of volcanic rocks based on the total alkali-silica diagram // J. Petrol. 1986. Vol. 27(3). P. 745–750.

30. *Ovalle J.T., La Cruz N.L., Reich M., Barra F., Simon A.C., Konecke B.A., et al.* Formation of massive iron deposits linked to explosive volcanic eruptions // Sci. Rep. [Internet]. 2018. Vol. 8(1). P. 14855. Available from: https://doi.org/10.1038/s41598-018-33206-3

31. *Corriveau L.* Iron oxide copper-gold (±Ag±Nb±P±REE±U) deposits: A Canadian perspective // Geol. Surv. Canada la Couronne. Québec, Canada, 2006. P. 1–23.

Submitted 26.01.2022
Accepted 18.02.2022

About the author

KOSTIN, Aleksey Valentinovich, Dr. Sci. (Geology and Mineralogy), chief researcher, Diamond and Precious Metals Geology Institute, Siberian Branch of the Russian Academy of Sciences, 39 Lenina pr., Yakutsk 677000, Russia,
http://orcid.org/0000-0002-5778-6505, e-mail: a.v.kostin2006@rambler.ru

Citation

Kostin A.V. Volcanic features of IOCG mineralization in Kildyam volcanic complex of Central Yakutia (Russia) // Arctic and Subarctic Natural Resources. 2022, Vol. 27, No. 1. P. 32–45. (In Russ.) https://doi.org/10.31242/2618-9712-2022-27-1-32-45